SCIENCE CHINA
Information Sciences

• RESEARCH PAPER •

June 2026, Vol. 69, Iss. 6, 162102:1–162102:15
https://doi.org/10.1007/s11432-024-4844-4

# Physiology-augmented multivariate temporal learning for adaptive simulation of electrical excitation in cardiac myocytes

Yuhang CHEN[1], Yacong LI[2], Jiahao CUI[1], Shuai LI[1*], Henggui ZHANG[2*], Aimin HAO[1] & Qinping ZHAO[1]

[1]*State Key Laboratory of Virtual Reality Technology and Systems, School of Computer Science and Engineering, Beihang University, Beijing 100191, China*
[2]*Life Simulation Research Center, Beijing Academy of Artificial Intelligence, Beijing 100085, China*

Received 27 June 2024/Revised 1 March 2025/Accepted 4 April 2025/Published online 19 May 2026

**Abstract** Cardiac electrophysiological modeling is an effective approach for investigating the mechanisms of arrhythmogenesis. So far, the mainstream of cardiac myocyte modeling depicts the electrophysiological properties of cardiac cells by using biophysically detailed differential equations to describe the activation and inactivation processes of ion channel dynamics. However, this approach is cumbersome and time-consuming to construct the mathematical representations for specific cases, impeding physiological adaptive modeling. Here, we introduce an innovative method called physiology-augmented multivariate temporal simulation (PAMTS), to rapidly and adaptively describe the cell-specific physiological behavior of cardiomyocytes. Based on the excitability of biological systems, PAMTS decouples cellular electric activity into external environmental influences and internal multivariate dynamic mechanisms. Then, the physiological information embedded in the mechanistic models is characterized as physiological templates that guide the complex dependencies across multi-physiological attributes, enabling stable and accurate prediction of future cellular physiological behavior. After systematically evaluating PAMTS in multiple electrophysiological modeling tasks, we demonstrate that PAMTS can be accurately and reliably applied to conduct adaptive modeling of the physiological behavior of various cell types. The study suggests that PAMTS has a promising potential to propel the development of personalized cardiac physiological models, which provide novel insights for rapid and adaptive modeling of complex physiological systems.

**Keywords** multivariate time-series prediction, adaptive modeling, deep learning, cardiac electrical activity, cellular computational model

**Citation** Chen Y H, Li Y C, Cui J H, et al. Physiology-augmented multivariate temporal learning for adaptive simulation of electrical excitation in cardiac myocytes. Sci China Inf Sci, 2026, 69(6): 162102, https://doi.org/10.1007/s11432-024-4844-4

## 1 Introduction

Cardiac arrhythmias and sudden cardiac death are among the leading causes of death worldwide [1]. Due to technical and ethical limitations associated with animal and human experiments, computational biology has concentrated on developing a detailed quantitative description of cardiac electrophysiology to validate and further explore arrhythmogenic mechanisms through computer simulations [2–4]. Computational models can simulate normal and pathological excitation and excitation propagation [5,6], enabling a detailed study on the mechanisms underlying the genesis of cardiac arrhythmias [7,8]. Moreover, the models can help to diagnose relevant cardiac diseases in advance and therefore prevent fatality via creating personalized cardiac electrophysiological digital twins [9,10].

In this work, we focus on the modeling of cell-specific electrical excitations, which subsequently enables the prediction of the electrical activity in the targeted pacing scenarios. This can assist researchers in unraveling the mechanism behind the corresponding physiological behaviors. In retrospect, numerous mathematical models consisting of ion channel currents have been developed [2,5,11–14]. These models can simulate physiological activities of ventricular cells [15–17]. With the continuous advancement of theoretical studies, the intricate interactions of multiple physiological components within the cell have progressively become explicit. However, the mathematical models have also become extremely complex, and even some models require more than 50 coupled differential equations to account for the complex dynamic behavior [11–14]. This results in the application of customized tasks, such as cell-specific physiological modeling and drug effects, being time-consuming and laborious. Researchers are required

* Corresponding author (email: lishuai@buaa.edu.cn, henggui.zhang@manchester.ac.uk)

 

to dedicate considerable time and effort to understand the differential equations, adjust the relevant mechanism parameters, and potentially integrate new mathematical descriptions compatible with the existing mechanisms.

Most recently, a more effective approach has been provided by deep time-series prediction models. These algorithms are intended to model dynamic behavior by summarizing the temporal patterns behind the data to predict the future system states, wherein the parameters are learned during the training of the deep neural network [18]. Numerous studies model physical systems from this perspective to replace the complex and time-consuming traditional methods, and have achieved promising performance [19–21]. However, there exist significant distinctions between physiological and physical systems, such as the excitability of cardiomyocytes and the complex coupling of multiple, distinct mechanisms during excitation. These differences impose new technical requirements on method design, feature extraction, and feature utilization. To the best of our knowledge, it remains extremely challenging to depict the electrical activity of ventricular cells based on deep time-series prediction methods and to ensure the stability of the simulations over long periods.

To address the aforementioned challenges, we propose physiology-augmented multivariate temporal simulation (PAMTS), a method that integrates physiological knowledge into multivariate time-series forecasting models. Specifically, our contributions can be summarized as follows.

- We introduce a novel data-driven framework for ventricular electrophysiology modeling that avoids the complexity of traditional approaches. Our method achieves high-fidelity predictions while maintaining long-term stability in physiological attributes.
- To enhance interpretability, we design a two-stage modeling strategy. In the first stage, prior physiological knowledge is used to construct physiological templates that provide a biologically relevant yet coarse approximation of cellular activity. In the second stage, a deep time-series forecasting model refines these predictions by capturing local fluctuations and fine-grained temporal patterns, leading to precise waveform reconstructions.
- Our method allows the pre-trained time-series model to be fine-tuned with a few electrophysiological data from a new cell type. This adaptability enables efficient prediction of physiological changes across different cellular conditions, making the approach broadly applicable.

## 2 Methods

### 2.1 Datasets

Due to ethical limitations and the absence of a generally accepted dataset of ventricular myocytes, we select the classical numerical cellular physiological model, the TNNP model [14], and the tailored model [22] considering pharmacology to establish a simulated dataset. As shown in Table 1, the dataset contains time series (TS) of endocardial cells, myocardial cells, and epicardial cells under normal conditions and under the influence of arsenic trioxide (ATO), which is a promising tumor therapeutic drug, for a total of 6 types of ventricular myocytes. Each TS comprises temporal changes in 18 physiological attributes (please refer to Table A1 in Appendix A).

The data for each cell-type consists of four sub-datasets corresponding to the training and testing of the action potential duration (APD) calculation module and the multivariate time-series decomposition module, extracting static temporal templates, and finally the test data for the overall method. The dataset for the APD calculation module and the multivariate time-series decomposition module both contain 15 TS, five for each pacing protocol. The training and test sets are divided in a 4:1 ratio according to the pacing protocols. Specifically, the uniform protocol represents the scenarios with constant stimulus frequency to obtain the steady-state electrical activity of the cells, the S1-S2 protocol is used to test the cellular response to sudden changes in the stimulus frequency, and the dynamic protocol is used to test the cellular response to gradual changes in the stimulus frequency. Both the S1-S2 protocol and the dynamic protocol can be used to obtain the cellular APD restitution (APDR). We prefer to calculate APDR by the S1-S2 protocol.

Data used to extract static temporal templates contains 4 TS under the uniform pacing protocol, corresponding to the training data part above. The test data for the overall method contains trajectories corresponding to each of the 3 pacing protocols. Unlike the dataset used for training and testing, this part of the data provides only the initial states of the cells and the stimulation protocols during the inference process. Then it is used as ground truth to validate the performance of architectural autoregressive prediction results.

Finally, unlike the numerical solving methods, the accuracy of the method is only related to the measurement accuracy of the data itself, independent of the predictive time-step. Therefore, the simulation data can be downsampled to significantly increase the time-step while maintaining accuracy. In this paper, we extend the time-step 50 times from 0.02 ms (the simulation step during data generation) to 1 ms to improve the efficiency of data ac-

**Table 1** Introduction to the dataset of ventricular cells used in this study. Datasets A and B are used for training and testing of the APD calculation module and the multivariate time-series decomposition module in a ratio of 4:1, respectively. Datasets C and D are not involved in training, where dataset C is used for preprocessing to get static temporal templates, and dataset D contains stimulus scenarios independent of the training data to test the inferential performance of the overall architecture. Notably, dataset D provides only the initial state of the cells and the stimulation protocol during inference. The symbol "/" is preceded by the data magnitude corresponding to endocardial and epicardial cells and followed by the data magnitude corresponding to myocardial cells. Furthermore, ATO can induce unstable electrical activity in cardiomyocytes under high-frequency stimulation. In this regard, we retain the TS data associated with high-frequency stimuli in pathological conditions to provide the corresponding change patterns and to investigate whether the model can learn relevant temporal patterns and infer physiological behaviors in novel scenarios.

| | | Uniform protocol | | | S1-S2 protocol | | | Dynamic protocol | | |
|---|---|---|---|---|---|---|---|---|---|---|
| | | #Configurations | #Step | #Beats | #Configurations | #Step | #Beats | #Configurations | #Step | #Beats |
| Normal condition | A | 5 | 2500 | 2500 | 5 | 18180/18145 | 18180/18145 | 5 | 20385/15315 | 20385/15315 |
| | B | 0 | – | – | 5 | 2450015 | 2565/2540 | 5 | 1450015/1300015 | 2600/2080 |
| | C | 4 | 2400012 | 800 | – | – | – | – | – | – |
| | D | 1 | 200003 | 200 | 1 | 490003 | 513/508 | 1 | 290003/260003 | 520/416 |
| Pathological condition (3 μM ATO) | A | 5 | 13750 | 13750 | 5 | 18130/18160 | 18130/18160 | 5 | 15305/13195 | 15305/13195 |
| | B | 55 | 1196305/1801305 | 2750 | 5 | 2450015/2500015 | 2540/2545 | 5 | 1300015/1150020 | 2080/1560 |
| | C | 4 | 2400012 | 800 | – | – | – | – | – | – |
| | D | 31 | 404581/609181 | 930 | 1 | 490003/500003 | 508/509 | 1 | 260003/230004 | 416/312 |

quisition while preserving the information contained in the waveform. To avoid data leakage between training and validation datasets, we grouped together TS acquired from the same stimuli amplitude and included these data either in the training or validation datasets.

## 2.2 Method architecture

The electrical activities of cardiomyocytes exhibit the all-or-none characteristic, and the external stimuli mainly serve as activators. Therefore, in terms of architecture design, our method decouples cellular physiological activities into two parts: (i) the influence of the external environment and (ii) the internal dynamic behavior, which are independently modeled using deep learning (DL) models. Due to the strong time-dependence of changes in cellular physiological attributes, we employ time-series prediction methods to describe the internal dynamic behavior. Moreover, these changes exhibit patterns at specific phases of excitation. We propose the scaling template-based strategy to instantiate this physiological knowledge and use it as prior temporal patterns to guide the subsequent prediction module to enhance prediction accuracy, stability over long iterations, and overall interpretability.

### 2.2.1 *The effect of pacing frequency on electrical activity*

Due to the slow recovery of ion channels or gradual accumulation of intracellular ion concentrations [23–25], the electrical activity of cardiac myocytes exhibits memory. Specifically, APD does not depend solely on the adjacent diastolic interval (DI), but on a longer history of DI values and the current cellular physiological state. To address this issue, we initially model the effect of stimulus current on membrane voltage and intracellular potassium concentration. Furthermore, we consider modeling the memory properties of electrical activity analogous to solving a regression problem. Therefore, PAMTS integrates the APD calculation module (Figure 1(a)) based on a fully connected neural network to implement the pre-calculation of APD upon receiving a stimulus. Given the performance and computational cost of the neural network, it consists of 12 fully connected layers with the hidden layers containing 32 neurons. The hidden layers are connected by rectified linear unit (ReLU) activation functions. The size of the input layer is determined by the reference adjacent DI and the number of defined physiological attributes. In the default settings, 3 adjacent history DIs are used to indicate the local stimulation protocol with 18 physiological attribute values to indicate the current cell state. The size of the output layer is 1, which corresponds to the APD value of the current stimulus.

### 2.2.2 *Representing the priori physiological knowledge as temporal patterns*

Due to the special properties and forms of physiological knowledge, it is admittedly often non-trivial to properly integrate the understanding of physical processes into the learning algorithms. The excitability of ventricular cells results in physiological attributes such as membrane voltage and ionic currents that exhibit patterns of change across excitation phases. Therefore, we adopt the strategy based on template deformation to instantiate the physiological knowledge embedded in the classical computational model and use it as temporal patterns to constrain subsequent timing prediction methods.

During the process of characterizing physiological knowledge, the first step is to extract the changes in each physiological attribute during excitation as the generic templates. To address this issue, we used the physiological model [14, 22] to fix the basic cycle length (BCL) for a period of simulation, allowing the model to reach the steady state with the chosen BCL. Then, the temporal changes in the physiological state during the steady state

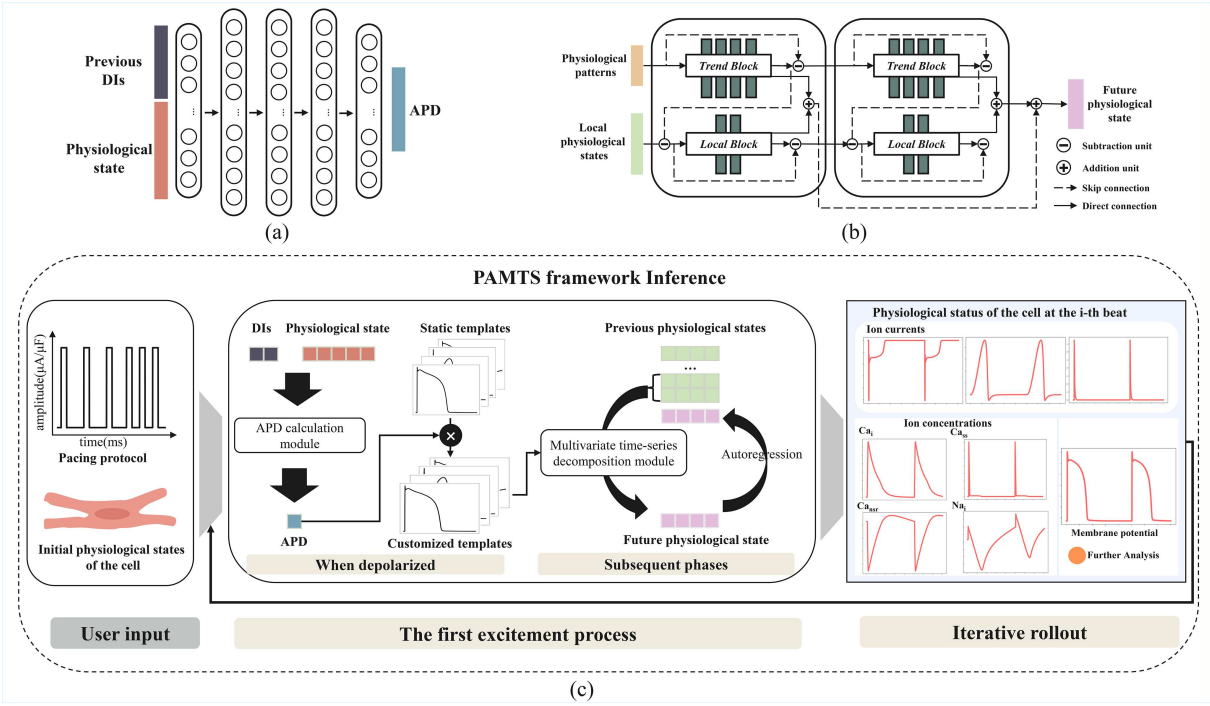


**Figure 1** (Color online) (a) Illustrative structure of the APD calculation module, which models the memory of cellular electrical activity; (b) illustrative structure of the multivariate time-series decomposition module for constructing the mapping function from localized historical states to future state guided by physiological patterns; (c) the PAMTS method enables the inference of the physiological behavior of cells in other situations through the combined use of the APD calculation module and the multivariate time series decomposition module.

are intercepted as static templates. The second step is to correct for the distribution shifts of templates between excitations under different conditions. Specifically, the static templates are rescaled in the time dimension to obtain the main oscillation frequency and the change trends of physiological attributes corresponding to a particular excitation. The specific process is as follows. After modeling the effect of pacing frequency on cellular physiological activity, we obtain the APD only at depolarization and use the ratio of this and the static APD to scale static templates yielding the tailored templates. Finally, since discrete storage is required, the tailored temporal template needs to be resampled after the scaling operation.

### 2.2.3 *The complex dynamic behavior induced by multiple distinct mechanisms*

In sharp contrast to conventional electrophysiological modeling methodologies, we present a novel approach that conceptualizes cellular electrical activity during excitation as a regularly sampled multivariate temporal prediction task. The changes in physiological attributes exhibit patterns during excitation, which can provide guidelines for temporal prediction methods. Therefore, we introduce the multivariate time-series decomposition module (Figure 1(b)), inspired by the work [26] on periodic time series forecasting. Briefly, it is an extended module based on residual learning that progressively decouples the contribution of the corresponding regions of historical observations and temporal templates to the future physiological state. Compared to the original work, our main contribution is to extend it from modeling univariate TS changes to multivariate TS prediction tasks and to abstract the all-or-none characteristic of excitation into trend information to provide guidance.

### 2.2.4 *Overview of the PAMTS method for analyzing physiological data*

PAMTS is an initiative effort to integrate physiological knowledge into the DL model, aiming to efficiently analyze physiological data and adaptively model the physiological behavior of ventricular cells. The framework operates in two distinct modes: training and inference. During training, PAMTS can either be fully retrained on the data-driven modules (APD computation module and multivariate time series decomposition module) using the target cell type datasets, or it can be fine-tuned on small target datasets using the pre-trained model. In inference mode, the modules of the framework work together to predict the electrical activity of target cells under specific pacing conditions based on user-defined inputs (please refer to Subsection 2.5).

Furthermore, PAMTS can be interpreted as a two-stage approach. (i) When a stimulus comes, the APD cal-

culation module predicts the APD corresponding to this excitation. The static template is then calibrated based on the scaling template strategy to yield the rough results of physiological states throughout the excitation period, whose slopes and amplitudes are often imprecise. (ii) The multivariate time-series decomposition module takes the rough results and the historical physiological states as inputs, predicts the corrected state at the next time-step, and employs autoregressive iterations to obtain the exact changes in multiple physiological attributes during excitation.

### 2.3 Data preprocessing

The values of cellular physiological attributes change over time, exhibiting strong temporal correlations. These signal values are typically recorded as the following uniformly sampled TS:

$$X = \{x_1, x_2, x_3, \ldots, x_{t-2}, x_{t-1}, x_t\}, \tag{1}$$

where $X$ denotes the entire continuous TS and $x_t$ indicates the physiological state of the cell at time $t$, which usually consists of multiple physiological attributes (Table A1 in Appendix A). Specifically, the time interval between two consecutive states depends on the user's requirements, which are set to 1 ms in this paper. Furthermore, biomarkers such as APD and DI corresponding to each excitation can be recorded from the physiological perspective. The APD referenced in this paper denotes APD90, calculated as described in [12], and the DI is the difference between the BCL and the APD. For the APD calculation module, the inputs are the DIs of the adjacent stimulus and the physiological state of the cell at depolarization, and the output is the APD.

For the multivariate time-series decomposition module, we process the TS based on the sliding window in order to convert it into applicable data. The sliding window consists of the look-back window and the forecast horizon. The look-back window provides historical observations as inputs, and as the window size gets larger, it contains more information, but increases the number of parameters in the model and decreases computational efficiency. The forecast horizon is used as the prediction target. The TS prediction models are to project the historical observations $x_{t-L:t} = [x_{t-L}, \ldots, x_{t-1}]$ into its subsequent future values $x_{t:t+H} = [x_t, \ldots, x_{t+H-1}]$:

$$x_{t:t+H} = f_\eta(x_{t-L:t}), \tag{2}$$

where $H$ is the length of the forecast horizon, $L$ is the length of the look-back window, $f_\eta$ is a mapping function parameterized by $\eta$. In this paper, we only set $L$ to 5 time-steps, which reduces the difficulty of acquiring data, due to the lower requirement of data continuity. Since the time of stimulus arrival is unpredictable at the cellular level, $H$ is set to 1. With the benefit of classical physiological models, the patterns of change in each physiological attribute during excitation are well characterized, which can provide guidance for the construction of implicit mathematical representations of historical physiological states to future states. Subsequently, the scaling template-based strategy is proposed to instantiate the above priori knowledge into comprehensible data $z$, which indicates the temporal patterns of each physiological attribute during a specific excitation. Therefore, Eq. (2) can be expanded to the following form:

$$x_{t:t+H} = f_\eta(x_{t-L:t}, z). \tag{3}$$

### 2.4 Method training

Our model consists of two separately trained DL modules optimized by the Adam optimizer. The initial learning rate is set to 0.001. The batch size is set to 2048. Then CosineAnnealingLR is used to reduce the learning rate (lr) gradually. The detailed reduction principle is as follows:

$$\mathrm{lr} = \mathrm{lr}_{\min} + \frac{1}{2}(\mathrm{lr}_{\max} - \mathrm{lr}_{\min})\left(1 + \cos\left(\frac{T_{\mathrm{cur}}}{T_{\max}}\pi\right)\right), \tag{4}$$

where $T_{\mathrm{cur}}$ and $T_{\max}$ represent the current number and the maximum number of epochs, respectively, $\mathrm{lr}_{\max}$ is the initial maximum learning rate, and in order to prevent a learning rate of 0, $\mathrm{lr}_{\min}$ is set to $10^{-9}$. Both networks are set to proceed in 200 epochs.

In general, our method requires only 7 h of training to enable both modules to reach convergence and accurately characterize the electrical activity of the cells. In training mode, PAMTS automatically constructs implicit mathematical representations of the corresponding physiological behavior through analyzing the available data. Thereafter, the user only needs to provide the initial states of the cells and the pacing protocol, which describes when the stimulus arrives to make subsequent inferences regarding cell-specific physiological behavior in other scenarios.

### 2.5 Method inference

In inference mode, the workflow of our method has changed, which is primarily reflected in the coupled use of individual modules that are modeled independently (Figure 1(c)). The user only needs to provide the initial physiological states of the cell, a protocol describing the stimulus, and the simulation duration to start the subsequent prediction. As shown in Algorithm 1, the overall simulation process is as follows. (i) When the stimulus comes, the APD calculation module predicts the APD for the current excitation. Subsequently, the temporal patterns of this stimulus are obtained by correcting the distributional offset of the static templates using the scaling template-based strategy. (ii) During the current excitation period, the historical state and the customized template are used as inputs to predict the physiological state of the next time step. The predicted cell state is then integrated into the history state sequence. Step (ii) is iteratively executed to achieve cyclic prediction throughout the current excitation period until either (iii) when a new stimulus arrives, re-execute (i), and then enter the loop corresponding to step (ii), or (iv) reach the endpoint of the user's preset stimulus protocol, thus terminating the simulation.

**Algorithm 1** The workflow of PAMTS in inference mode.

**Input:** Initial history of physiological states $S_0 = [x_{-L}, \ldots, x_{-1}]$, where $x_t \in \mathbb{R}^d$ denotes physiological attributes at t, static template $\mathcal{Z}_{\text{base}}$, stimulation protocol $\mathcal{P} = \{(t^{(i)}, )\}_{i=1}^{N}$, end time $T_{\text{end}}$.
**Output:** Predicted sequence of cellular states $\mathcal{H} = [x_0, \ldots, x_{T_{\text{end}}}]$.

$t \Leftarrow 0$, $\mathcal{H} \Leftarrow S_0$, $i \Leftarrow 1$;
**while** $t < T_{\text{end}}$ **do**
  **if** $t == t^{(i)}$ **then**
    Predict APD: $\text{APD}^{(i)} \Leftarrow$ `APD_calculation_module`$(I^{(i)}, \mathcal{H})$;
    Generate custom template: $Z^{(i)} \Leftarrow$ `Scaling_template-based_strategy`$(\mathcal{Z}_{\text{base}}, \text{APD}^{(i)})$;
    $i \Leftarrow i + 1$;
  **end if**
  Prepare input: $\mathcal{X}_t \Leftarrow \left(\mathcal{H}_{t-L:t}, Z^{(i-1)}_{t-L:t+1}\right)$;
  Predict next state: $x_t \Leftarrow$ `Multivariate_time-series_decomposition_module`$(\mathcal{X}_t)$;
  Append $x_t$ to $\mathcal{H}$;
  $t \Leftarrow t + 1$;
**end while**

### 2.6 Performance evaluation

In the default setting, we provide modeling tasks for a total of six physiological systems: endocardial cell, myocardial cell, and epicardial cell under normal conditions and the influence of the tumor treatment drug ATO. Furthermore, the test experiments included prolonged prediction of cellular physiological states in multiple pacing protocols and an important physiological property, APDR, which plays a crucial role in assessing the stability of cardiac electroactivity and the risk of arrhythmias.

Furthermore, we use agreement metrics in the field of TS prediction, such as R-squared ($R^2$), mean absolute percentage error (MAPE), and normalized deviation (ND) to evaluate the performance. The specific formulas are as follows:

$$R^2 = 1 - \frac{\sum_{i\in\Omega}(y_i - \hat{y}_i)^2}{\sum_{i\in\Omega}(y_i - \bar{y})^2}, \tag{5}$$

$$\text{MAPE} = \frac{1}{|\Omega|}\sum_{i\in\Omega}\left|\frac{y_i - \hat{y}_i}{y_i}\right| \times 100\%, \tag{6}$$

$$\text{ND} = \frac{\sum_{(i,j)\in\Phi}|x_i^j - \hat{x}_i^j|}{\sum_{(i,j)\in\Phi}|x_i^j|}. \tag{7}$$

In (5)–(7), $\hat{y}_i$ represents the predicted value of the $i$th sample in the APD evaluation space $\Omega$, which is not involved in training, and $y_i$ represents the corresponding ground truth. $\Phi$ represents another evaluation space for measuring the accuracy of inference to physiological trajectories by PAMTS, where $x_i^j$ and $\hat{x}_i^j$ represent the ground truth and the corresponding predicted value, respectively. Since the cell state consists of multiple electrophysiological attributes, $j$ is used to represent the attribute index.

### 2.7 Hardware and software for data analysis

All the data analysis procedures presented in this work were performed on an Asus desktop with an Intel Core i7-10700@ 2.9 GHz 8-core CPU, 16 GB Kingston RAM, and an NVIDIA GeForce RTX 3060 GPU. All processing

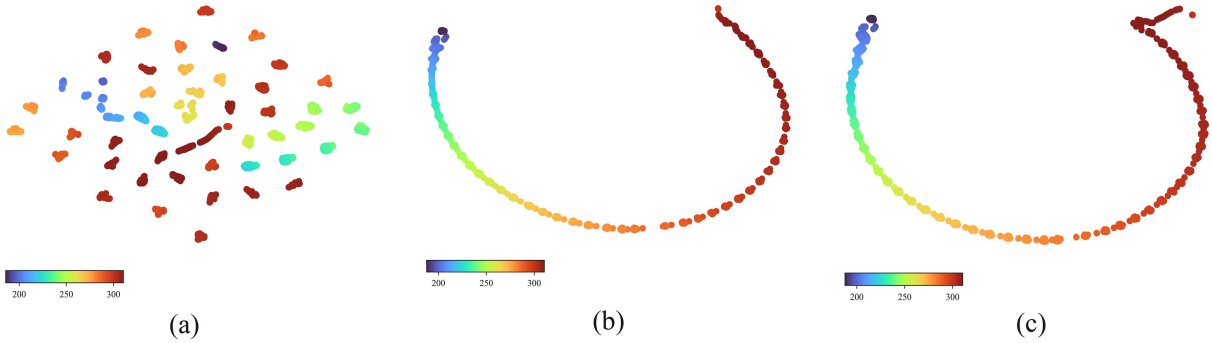


**Figure 2** (Color online) T-SNE dimensionality reduction of physiological patterns corresponding to different stimuli. The color indicates the APD value of the corresponding stimulus. (a) Overall training set; (b) one continuous pacing trajectory in the training set; (c) the corresponding continuous trajectories obtained from the scaling template-based strategy.

**Table 2** Performance of the APD calculation module.

| | #test_sample | $R^2$ (%) | MAPE (%) |
|---|---|---|---|
| Uniform protocol | 500 | 98.336 | 0.058 |
| S1-S2 protocol | 3636 | 99.463 | 0.089 |
| Dynamic protocol | 4077 | 99.992 | 0.081 |
| Average | – | 99.264 | 0.076 |

steps, including network training and validation, were carried out under PyTorch software libraries. Time-series processing and data analysis were carried out using Python language.

## 3 Results

### 3.1 Performance in modeling cellular electrical memory and characterizing physiological patterns

The changes in pacing frequency affect cellular electrical memory. To verify the effectiveness of PAMTS in this task, we integrate physiological trajectories under multiple pacing protocols to obtain complex pacing datasets as test datasets to evaluate the performance under these conditions.

As shown in Table 2, we firstly employ $R^2$ to evaluate the fitting to the actual data, and our model achieves 99.264% across all the tested samples, indicating that PAMTS can accurately capture the underlying pattern in the data. MAPE is then used to evaluate the accuracy of the APD predicted by PAMTS. The MAPE of the PAMTS is 0.076%, indicating that PAMTS is effective in predicting APD under different scenarios (please refer to Figure A1 in Appendix A for prediction curves under multiple test scenarios).

At a specific phase of action potential (AP), membrane voltage, ionic currents, etc., exhibit patterns of change, which can provide significant guidance for modeling the internal dynamic behavior. Classical physiological models have been able to accurately demonstrate the physiological patterns of each physiological attribute under different stimulus conditions. However, as macroscopic information about physiological processes, it needs to be instantiated as comprehensible data before use. For this purpose, we propose the scaling template-based strategy to represent the aforementioned physiological patterns.

The template, having a high similarity to the pacing data in terms of characterizing the direction of change, should be deemed successful. Therefore, to assess the quality of the representation, we firstly encode the changes in each electrophysiological attribute during excitation as a set of binary data, where encoding a positive gradient as 1 and the opposite as 0. Then, we calculate the Hamming distance (i.e., the number of differences between the two sequences in the direction of the representational changes) between the original data and the template to quantitatively analyze the performance of the strategy. The results obtained confirm the validity of our proposed approach. More specifically, we calculate the Hamming distances of 5 consecutive physiological data with a total of 2590 beats and their corresponding custom templates and find that the customized templates can accurately characterize the periodicity with the bit error rate (BER) of only 1.442%.

Additional qualitative experiments are conducted to validate the strategy to represent physiological patterns in PAMTS. We use t-distributed stochastic neighbor embedding (t-SNE) to visualize the mapping results of binary data representing temporal patterns. The corresponding results reveal that pacing samples with similar APDs form independent clusters, while samples with larger differences are distinguished (Figure 2(a)). Notably, we randomly

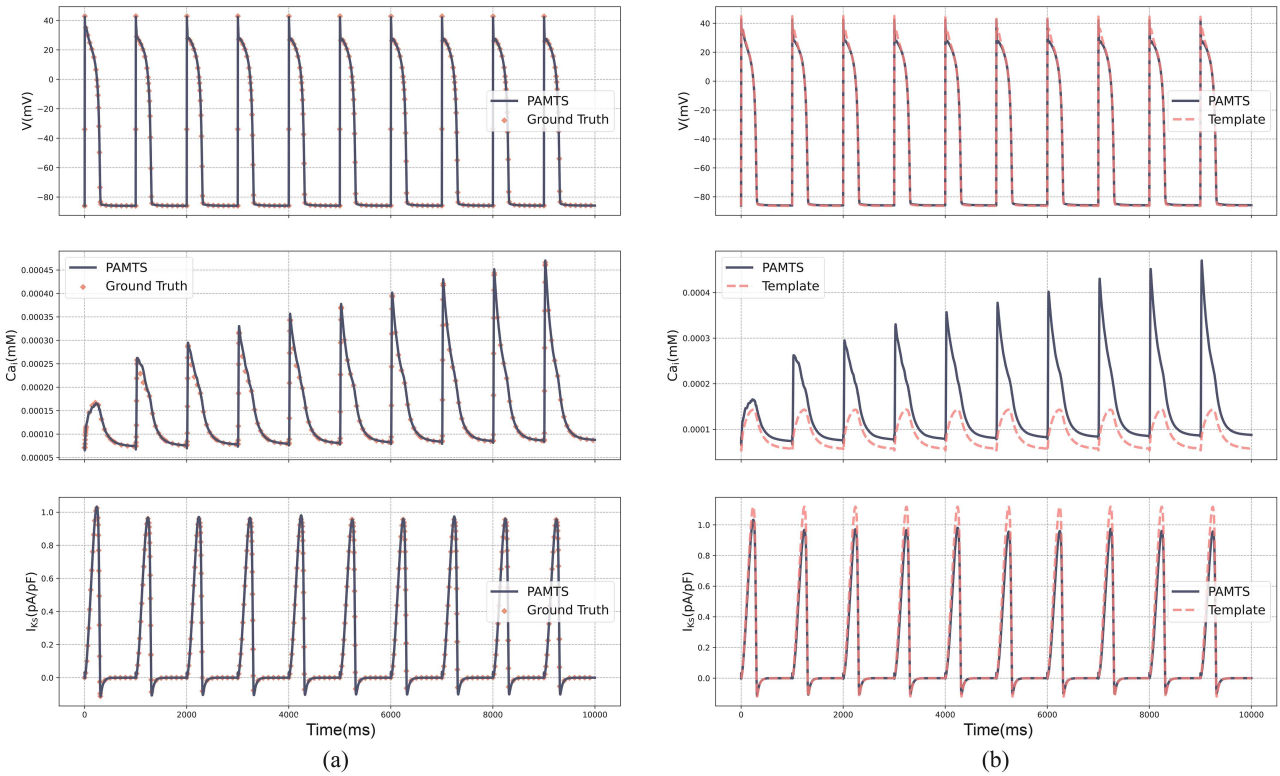


**Figure 3** (Color online) (a) The predicted results of AP, calcium transients, and $I_{\mathrm{Ks}}$ during 10 consecutive beats (pacing frequency 1 Hz) obtained by PAMTS; (b) the difference between the final prediction results and temporal templates for the corresponding attributes.

visualize a continuous pacing trajectory and the corresponding temporal template, and find a nearly consistent result after dimensionality reduction, suggesting that they may have similar local structure and relative distance relationship in high-dimensional space (Figures 2(b) and (c)). In conclusion, the scaling template-based strategy enables PAMTS to characterize the temporal changes of physiological attributes during excitation under various conditions.

Based on the functions described above, PAMTS can accurately model the memory of cellular electrical activity and represent physiological knowledge from classical physiological models as temporal patterns. In non-autoregressive form, the forecast horizon of the multivariate time-series decomposition module is 1, which does not help to demonstrate its performance on its own. Therefore, we demonstrate the performance of the overall method with subsequent validation experiments in inference mode.

### 3.2 Performance of the PAMTS method in inferring the electrical activities in three types of ventricular cell

In inference mode, we initialize the cell state and then perform long-term iterative predictions for PAMTS based on multiple pacing protocols and compare the results to the ground truth. Notably, the different electrophysiological attributes vary greatly in scale, with some attribute values extremely close to zero. In such cases, the MAPE metric can be severely distorted. Therefore, we adopt ND as the metric to eliminate the effect of order-of-magnitude differences between attributes and to comprehensively demonstrate the performance for adaptive modeling of cellular electrical activity by PAMTS.

We first verify the dynamic behavior generated by PAMTS corresponding to the physiological properties of endocardial cells at 1 Hz pacing frequency. The results obtained confirm the validity of our proposed approach. The overall cellular ND for a single steady beat is only 3.112%, indicating that PAMTS can accurately model changes in a total of 18 physiological attributes during excitation. We apply PAMTS to a scenario with constant stimulus frequency (pacing period of 1000 ms, total of 65 consecutive beats), and achieve high accuracy with an overall cell system ND of 3.231% during the entire stimulation process. As shown in Figure 3(a), the physiological attributes corresponding to different beats would be shifted and even the waveforms would be changed when converging to the steady state. However, the ND of continuous pacing does not rise significantly compared to the single steady stimulation, verifying the stability of the overall architectural design in the autoregressive iterative prediction

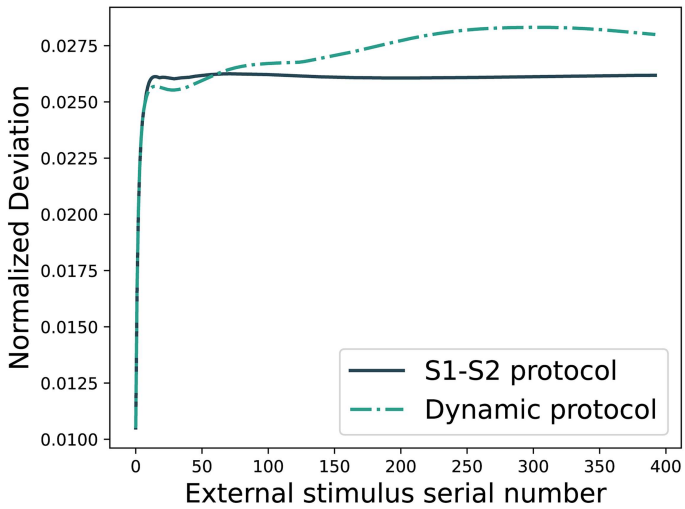


**Figure 4** (Color online) Normalized deviation curve between PAMTS inference of cell physiological behavior and ground truth during two complex pacing protocols (400 beats).

process. Then we visualize the final output of the model and temporal templates, which represent physiological knowledge. The templates demonstrate substantial differences from the final predictions in terms of amplitude and gradient (Figure 3(b)). However, they characterize the main oscillation frequency and the change trends of physiological attributes during each excitation, providing guidance on how the model can refine the final prediction based on local states.

We further perform validation experiments in independent complex pacing scenarios to demonstrate that PAMTS can effectively infer the implicit property of electrical activity—APD restitution (APDR), which plays a crucial role in the assessment of cardiac electrical activity stability and arrhythmia risk. More specifically, we use PAMTS to predict the corresponding physiological behavior in the case of suddenly altering the coupling interval between two consecutive beats (S1-S2 pacing protocol) and gradually shortening the pacing cycle length (dynamic pacing protocol). Our results show that PAMTS achieves an average $R^2$ of 98.989% (S1-S2 protocol: 99.782%, dynamic protocol: 98.197%) and an MAPE of 0.658% (0.490% for S1-S2 protocol, 0.826% for dynamic protocol, please see Figure A3 in Appendix A for more information on APDR curves obtained by two pacing protocols). Further analysis of the overall error reveals that ND changes for both pacing protocols show a "warm start" phenomenon, in which the error increases rapidly during the initial phase and then gradually decreases to a stable position in the subsequent phase. This initial phase indicates that the cells are adjusting to the new environment and gradually transition from the initial state to a stable state corresponding to the environment. The phase is more drastic and constitutes a smaller proportion of the training data, which makes it more difficult to predict. During the dynamic pacing protocol, the error rebounds much more before the end of the simulation. Probably because there is less training data for the small pacing periods, the model predicts the dynamic behavior of the latter half of the continuous rapid excitation phase with inferior accuracy, but the average heartbeat ND eventually stabilizes below 3.00% (Figure 4).

In addition to endocardial cells, cardiomyocytes include myocardial cells and epicardial cells. They have differential biological characteristics such as ion channel current densities and AP profiles, due to the intrinsic differences in their electrophysiological properties. To verify the universal applicability of the PAMTS framework, we apply it to the specific modeling of two other cardiomyocytes. The specific experimental results are shown in Table 3, and PAMTS achieves accurate inference of electrical activity in all test scenarios.

In conclusion, the aforementioned physiological experiments demonstrate that the PAMTS architecture is extraordinarily effective in efficiently analyzing data and adaptively achieving complex dynamics behavior modeling of cells. Moreover, it is capable of accurately and stably reproducing the detailed characteristics of cellular electrical activity in long-time simulations that are not covered by the training data.

### 3.3 Validation of the method in reproducing drug effects on cellular electrical activities

In the presence of drugs, intracellular conductance channels and ion balance may be significantly affected, which results in abnormal electrical activity. Rapidly analyzing relevant physiological data and describing the physiological activity of cells under the influence of drugs can improve the efficiency of drug development and ensure the safety

**Table 3** Performance of the method for inferring electrical activities in three types of ventricular cells, consisting of sub-module tests and cellular tests.

| | Metric | Endocardial cell | Myocardial cell | Epicardial cell | Average |
|---|---|---|---|---|---|
| APD calculation module | $R^2$ (%) | 99.264 | 99.900 | 99.643 | 99.602 |
| | MAPE (%) | 0.076 | 0.044 | 0.063 | 0.061 |
| The scaling template-based strategy | BER (%) | 1.442 | 2.582 | 5.300 | 3.108 |
| Independent uniform protocol for method evaluation | ND rollout-1 beat (%) | 2.519 | 1.282 | 1.130 | 1.644 |
| | ND rollout-65 beats (%) | 3.231 | 1.832 | 1.917 | 2.327 |
| | ND of steady beat (%) | 3.112 | 0.959 | 2.118 | 2.063 |
| Independent S1-S2 protocol for method evaluation | ND rollout-all beats (∼460) (%) | 3.342 | 1.706 | 2.161 | 2.403 |
| | $R^2$ of the APDR (%) | 99.772 | 99.682 | 99.500 | 99.651 |
| | MAPE of the APDR (%) | 0.475 | 0.497 | 0.564 | 0.512 |

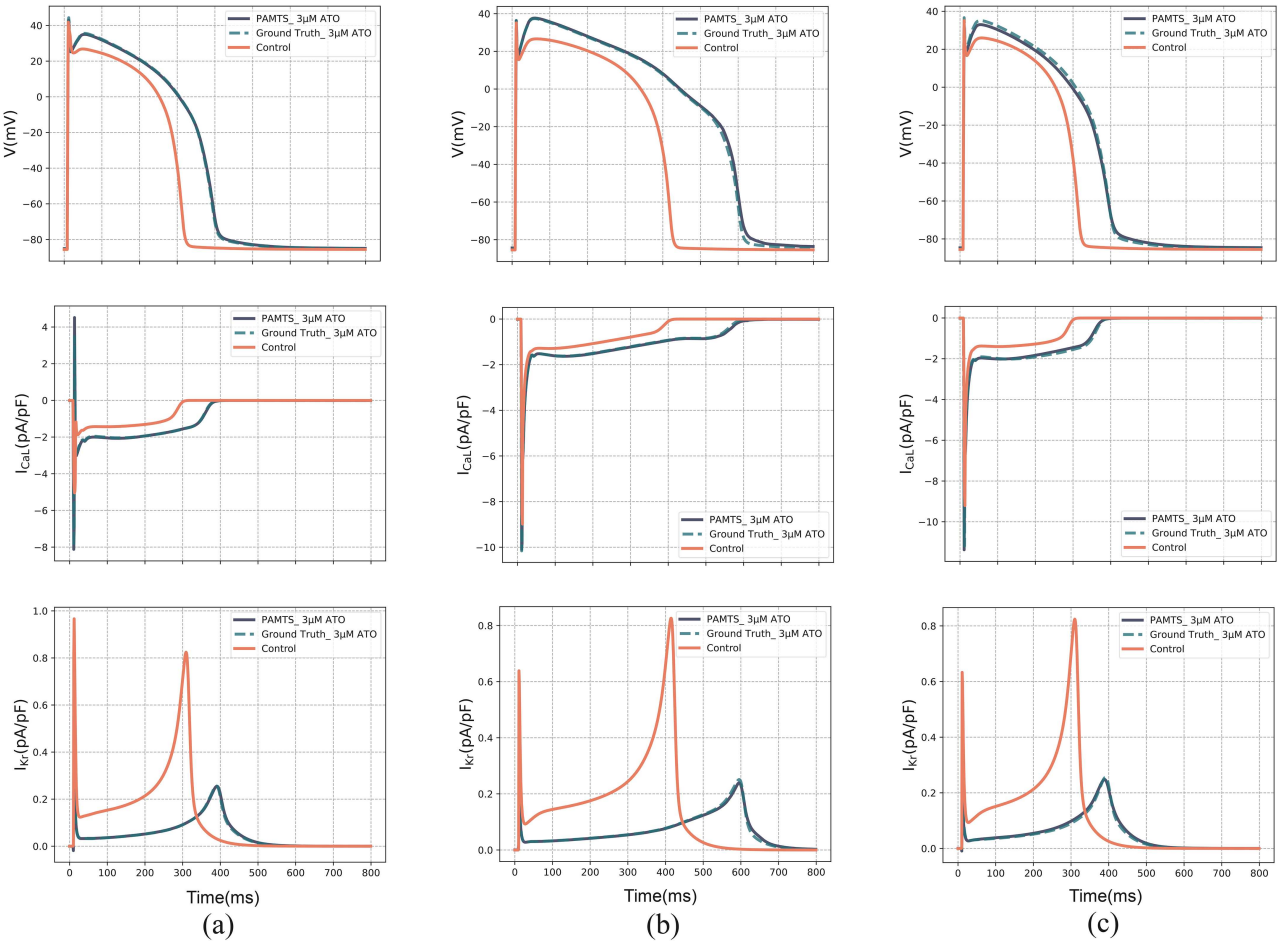


**Figure 5** (Color online) The impact of 3 μm ATO on physiological attributes of different ventricular myocytes. (a) Endocardial cell; (b) myocardial cell; (c) epicardial cell.

of clinical application [4, 22, 27, 28]. To demonstrate the auxiliary analysis capabilities of PAMTS, we apply it in a customized task designed to help researchers explore the effects of ATO on cardiomyocytes.

Based on relevant clinical observations, ATO primarily impacts the rapid delayed rectifier potassium current ($I_{\mathrm{Kr}}$), as well as L-type calcium ($I_{\mathrm{CaL}}$) channels to induce cardiotoxicity. In this regard, we first utilize PAMTS to predict the changes in partial physiological attributes of three distinct cardiomyocyte types under 1 Hz pacing frequency. We find that ATO leads to a decrease in $I_{\mathrm{Kr}}$ and an increase in $I_{\mathrm{CaL}}$, and thus prolongs APD in cardiomyocytes to different degrees (Figure 5), consistent with [22, 29]. Notably, the rate of APD prolongation varied (endocardial cell: 29.434%, myocardial cell: 44.924%, epicardial cell: 31.209%) among different cell types, exacerbating the heterogeneity. Moreover, the cellular APD ratios of these types change from 1.000:1.346:1.003 to

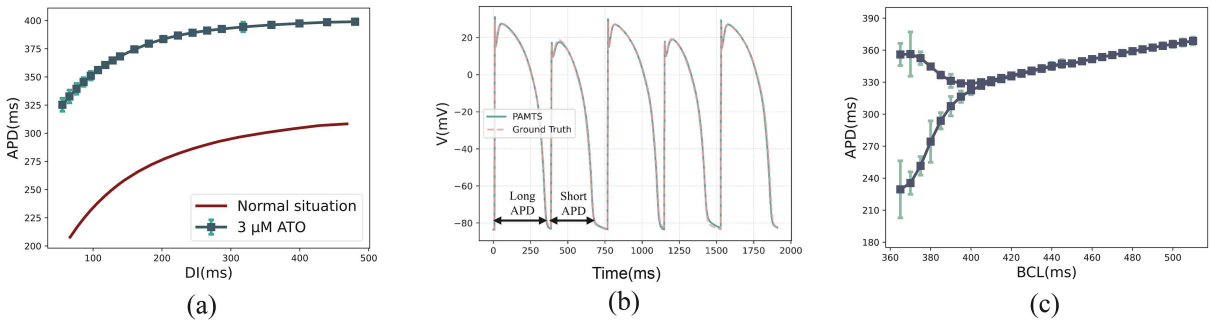


**Figure 6** (Color online) (a) The restitution curves of epicardial cell under the influence of 3 μm ATO; (b) ATO induces alternans in the electrical activity of epicardial cell; (c) the main phenomenon of alternans is the alternation of the corresponding long and short APD membrane voltages at a fixed pacing frequency. The bifurcation of the restitution curves indicates the presence of two APDs in a single BCL.

**Table 4** Performance of the method for inferring electrical activities in three types of ventricular cells under the influence of 3 μm ATO, consisting of two types of cellular tests.

| | | Endocardial cell | Myocardial cell | Epicardial cell | Average |
|---|---|---|---|---|---|
| Independent | ND of (∼460) beats (%) | 4.817 | 9.220 | 6.278 | 6.772 |
| S1-S2 protocol | $R^2$ (%) | 98.039 | 89.278 | 98.384 | 95.234 |
| for method evaluation | MAPE (%) | 0.631 | 1.803 | 0.637 | 1.024 |
| Independent uniform protocol with gradually shortening BCL | MAPE of alternans (%) | 1.807 | 0.863 | 1.390 | 1.353 |

1.000:1.507:1.016, potentially increasing the risk of ventricular tissue arrhythmias.

The APDR curve reflects the ability of cells to adapt to frequency changes. Therefore, we apply PAMTS to predict the impact of 3 μm ATO on the APDR curves of cardiomyocytes based on the S1-S2 pacing protocol. The experimental results demonstrate that the APDR curves for all three types of cells exhibit different degrees of the upward shift to the right and increase in slope (Figure 6(a)). This confirms that the cardiomyocytes cannot sustain high-frequency pacing activity under the influence of ATO, leading to a decrease in the stability of the electrical activity [22, 30, 31]. As shown in Table 4, PAMTS achieves high accuracy in reproducing three cellular APDR characterization under pharmacological conditions with an average cellular MAPE of only 1.024%. In an analysis of cellular ND changes during 460 consecutive pacing sessions, PAMTS achieves a stable and accurate prediction, with the average ND eventually stabilizing below 9.20%. Moreover, we suggest that the high ND in myocardial cells may be directly caused by the slightly suboptimal performance of the APD calculation module, which results from a smaller total number of pacing in the pacing trajectories, or a slight mismatch in the hyperparameters.

To investigate ATO-induced electrical activity of cells under high-frequency stimulation, we establish uniform protocols with progressively shorter BCLs and analyze the corresponding physiological behavior of the cells predicted by PAMTS. In normal conditions, even if the BCL is small, the APDs corresponding to adjacent excitations do not fluctuate dramatically. As shown in Figure 6(b), PAMTS infers that alternation occurs in cellular electrical activity, consistent with the findings of existing research [22, 32, 33]. This suggests that the cardiotoxicity of ATO may be reflected in the instability of electrical activity under high-frequency stimulation. Furthermore, the model achieves high accuracy in predicting the pattern of APD changes under different BCLs with a cell-averaged MAPE of 1.353% (Figure 6(c), Table 4).

Overall, the results indicate that PAMTS can be extended to rapidly describe the physiological behavior of ventricular cells in the presence of drugs. This capability can facilitate researchers in probing drug effects and screening drugs that exert less impact on cardiac electrical activity, with promising value for application.

### 3.4 Impact of target data availability and noise level on the fine-tuning performance of pre-trained models

This subsection evaluates the impact of limited target cell data and measurement noise on the performance of our proposed method. We conducted fine-tuning experiments using three data proportions (2.14%, 3.20%, and 4.27% of the training set) and two levels of Gaussian noise (2.5% and 5.0%) across three target cell types. To assess the effect of fine-tuning data quantity, we used the PAMTS model trained on endocardial cells (Subsection 3.2) as a pre-trained model. We then fine-tuned it using data from epicardial cells, myocardial cells, and epicardial cells exposed to 3 μm ATO. The model was fine-tuned with 50 (2.14%), 75 (3.20%), and 100 (4.27%) pacing cycles of

**Table 5** Effect of fine-tuning data amount and noise levels on model prediction accuracy for different target cell types.

| Target cell type | Metric | Epicardial cell (normal) | | | Myocardial cell (normal) | | | Epicardial cell (3 μm ATO) | | |
|---|---|---|---|---|---|---|---|---|---|---|
| Data ratios | | 2.14 (%) | 3.20 (%) | 4.27 (%) | 2.14 (%) | 3.20 (%) | 4.27 (%) | 2.14 (%) | 3.20 (%) | 4.27 (%) |
| Scenario 1 | ND (%) | 11.28 | 11.52 | 4.92 | 14.63 | 14.85 | 8.02 | 15.52 | 12.79 | 6.13 |
| Scenario 2 | ND (%) | 9.08 | 6.36 | 3.97 | 13.98 | 12.62 | 8.31 | 10.77 | 10.68 | 5.51 |
| Scenario 3 | ND (%) | 10.69 | 8.72 | 7.00 | 16.37 | 15.69 | 10.99 | 16.07 | 13.92 | 10.45 |
| Noise ratios | | 0.00 (%) | 2.50 (%) | 5.00 (%) | 0.00 (%) | 2.50 (%) | 5.00 (%) | 0.00 (%) | 2.50 (%) | 5.00 (%) |
| Scenario 1 | ND (%) | 4.92 | 7.47 | 12.95 | 8.02 | 10.51 | 15.69 | 6.13 | 6.79 | 12.56 |
| Scenario 2 | ND (%) | 3.97 | 6.61 | 13.66 | 8.31 | 10.76 | 13.58 | 5.51 | 9.57 | 11.07 |
| Scenario 3 | ND (%) | 7.00 | 9.90 | 12.67 | 10.99 | 12.40 | 16.46 | 10.45 | 11.38 | 12.84 |
| Variance | | 1.60 | 1.94 | 0.17 | 1.79 | 0.70 | 1.48 | 4.83 | 3.56 | 0.60 |

target cell data recorded at a 1000 ms pacing interval. We then evaluated its predictive performance under three conditions: the next 20 pacing cycles at 1000 ms, the first 20 cycles at 800 ms, and the first 20 cycles at 600 ms.

Results (Table 5) indicate that fine-tuning with a small amount of target cell data significantly maintained the ability of the model to predict physiological responses under different pacing conditions, with prediction errors within 15%. Performance improves as the amount of fine-tuning data increases. Notably, the improvement from 3.20% to 4.27% is more substantial than from 2.14% to 3.20%, suggesting a possible threshold where target cell data yields greater accuracy gains. Prediction errors are higher for target cell types that differ more biologically from the source cell type. With the same amount of data, epicardial cells show lower errors than myocardial cells and epicardial cells exposed to 3 μm ATO. This indicates that models require more data to adapt to physiologically distinct target cells, emphasizing the need for larger fine-tuning datasets when applying pre-trained models to biologically diverse cell types.

To evaluate model robustness against measurement noise, we incorporated simulated noise into the fine-tuning data. Using 100 pacing cycles of target cell data with 2.5% and 5.0% Gaussian noise, we assessed performance under the same three pacing conditions. Our results show that the model maintains a degree of robustness, demonstrating its potential for real-world applications where experimental data may contain errors. However, as expected, noisy data degrades overall performance while improving model stability. Biological differences among cell types continue to influence adaptation under noisy conditions.

Overall, our findings suggest that fine-tuning with a small amount of new data allows the pre-trained model to generalize across different cell conditions. However, substantial biological differences between cell types may necessitate additional training with larger datasets to achieve optimal performance.

## 4 Discussion

So far, the workflow of constructing the electrophysiologic mechanisms in ventricular cells has frequently been based on the Hodgkin-Huxley model or Markov model to describe ion channel dynamics, then considering biophysical principles to select key physiological parameters and establish the corresponding mathematical equations, finally fitting the data to determine parameter values [2,11–14]. This method is effective but laborious and time-consuming imposing high demands on researchers in terms of physiological knowledge accumulation, data analysis skills, and the level of mathematical modeling. In addition, its parameter calibration is usually done manually using subjective validation criteria for the specific task [34, 35]. It is anticipated that data-driven DL techniques will alleviate the aforementioned issues. However, it is extremely difficult to model highly nonlinear electrophysiological systems and assure the stability of long-term simulations.

In this study, we present PAMTS, a DL approach based on physiological knowledge that can rapidly analyze physiological data and adaptively describe cellular electrical activity. It divides the complex physiological behavior of cells into external environmental influences and internal dynamic behavior and automatically constructs mathematical representations using DL models, respectively. Then, it expresses the domain knowledge from the classical physiological model as time-ordered physiological patterns, constructs the connection between the two parts, and improves the performance and interpretability of the overall architecture. Furthermore, the method can be interpreted as a two-stage approach: (i) according to the excitability of the cardiomyocytes, scaling the physiological template to obtain rough results; (ii) analyzing local information to obtain precise results using the multivariate time-series decomposition module. Finally, the PAMTS method is open source and subsequently available at the

website[1)].

In terms of validation, we evaluate the performance of the method to model the physiological behavior of ventricular cells under normal and pathological conditions, respectively. We first verify that the APD calculation module is able to accurately predict the effects of stable, abruptly changed, and progressively changed stimulus frequencies on electrical activity. Then, the performance of the scaling template-based strategy to characterize the physiological patterns of various cell types is demonstrated by quantitative and qualitative analyses. In the inference mode, physiological experiments demonstrate that our method can predict the physiological behavior of cells under untrained situations. It is able to accurately and stably infer multiple ventricular cellular APs, ionic currents, ionic concentrations, and electrophysiological properties APDR under normal conditions. Furthermore, we apply the PAMTS to model the effect of the tumor therapeutic drug ATO on the electrical activity of ventricular cells, accurately reproducing the phenomenon of alternans, indicating that this method may be useful for exploring the potential effects of the drug on cardiac function.

PAMTS possesses several novelties and advantages over existing approaches [2, 36]. First, contrary to numerical approaches, the prediction precision of the method is only related to the measurement precision of the data itself, not to the time step. Furthermore, we propose an adaptive modeling method that enables rapid analysis of available physiological data to describe the corresponding cellular electrical activity without cumbersome manipulation. Furthermore, compared with the classical physiological models from the first principles, we start from the qualitative traits of biological systems called the all-or-none characteristic and represent it as temporal patterns of different physiological attributes during excitation. Then, it is integrated into the method to improve the overall performance and interpretability. To the best of our knowledge, we make a pioneering endeavor to explicitly incorporate the macro-physiological property into multivariate time-series prediction methods for rapid and adaptive modeling of cellular electrical activity.

**Limitations and future studies.** To the best of our knowledge, we do a preliminary exploration of a DL-based approach for rapid and adaptive modeling of physiological behavior in ventricular cells with some limitations.

PAMTS has been extensively tested using classical mechanistic models, but its effectiveness in real physiological settings remains unverified. While some cardiac physiological datasets exist [37–39], most are clinical, such as ECG recordings, and do not provide direct intracellular electrophysiological measurements. Moreover, high-quality experimental data remain scarce. To address this issue, future work will focus on collaborating with physiology laboratories to integrate literature data and experimental data to construct datasets with multiple electrical remodeling phenomena for comprehensive, real-world validation. In addition, while mechanistic models describe ion channel kinetics and cellular interactions, offering direct physiological interpretations, PAMTS primarily predicts behavior without providing detailed mechanistic explanations. To enhance interpretability, future research will explore embedding biophysical constraints, such as physics-informed loss functions inspired by equivalent circuit models, and incorporating neural network structures based on physiological principles. Although the calibration phase in PAMTS effectively reduces template-related biases, areas of rapid physiological change remain sensitive to the initial template scaling. This constraint can impact prediction accuracy, particularly during sharp transitions in cellular activity. Future work will aim to enhance the model's generalization and calibration capabilities by improving how local dynamic adjustments are handled in these critical regions. This will help ensure more accurate and reliable predictions, even in complex physiological scenarios. Furthermore, while fine-tuning with limited data can adapt PAMTS to new conditions, significant biological differences between cell types may still require more data to fine-tuning, limiting its generalizability. To overcome this problem, future work will focus on optimized experimental protocols and advanced transfer learning strategies such as multi-task learning and meta-learning, in order to better capture cellular physiological properties using minimal data. These approaches aim to enhance knowledge transfer efficiency, which is particularly valuable for studying rare cardiac diseases where data availability is limited. Lastly, PAMTS is currently designed to analyze laboratory-generated data and support physiological research. Expanding its application to clinical settings could offer valuable insights for personalized cardiac modeling. In future work, we aim to integrate it with clinical data, such as ECGs, to develop personalized digital twins for risk assessment and treatment planning.

## 5 Conclusion

In this work, we propose PAMTS, a DL method that integrates physiological knowledge and enables end-to-end modeling of cellular electrical activity from the TS prediction perspective. Effectively, our solution consists of a novel integration that instantiates physiological knowledge embedded in existing classical models as temporal templates

1) https://github.com/Minghuang-Chen/PAMTS.

to provide guidelines for DL models to facilitate the refinement of inference results. For experimental validation, we first verify the module performance and the rationality of the pathway based on the all-or-none characteristic of excitation, then demonstrate the accuracy and stability of PAMTS in the inference of multiple cellular physiological behavior in novel scenarios and efficiently reproduce the implicit physiological property, APDR by our method. Furthermore, we show that PAMTS can facilitate the exploration of changes in cellular electrical activity in drug-induced effects. Based on powerful data analysis capabilities, PAMTS rapidly constructs tailored mathematical representations, providing promising avenues for achieving adaptive modeling of complex biological systems. In addition, the phenomenological model, it is used to predict the changes of multiple physiological attributes under multiple pacing scenarios, which gives reference to the analysis of cellular electrical activity and drug development.

**Acknowledgements** This work was supported in part by National Key Research and Development Program of China (Grant No. 2023YFF1203803), National Natural Science Foundation of China (Grant Nos. 62102036, 62501038), Beijing Science and Technology Plan Project (Grant No. Z231100005923039), and Beijing Natural Science Foundation (Grant No. L242141).

**Supporting information** Appendix A. The supporting information is available online at info.scichina.com and link.springer.com. The supporting materials are published as submitted, without typesetting or editing. The responsibility for scientific accuracy and content remains entirely with the authors.

**References**

1 Tsao C W, Aday A W, Almarzooq Z I, et al. Heart disease and stroke statistics 2023 update: a report from the American Heart Association. Circulation, 2023, 147: e93
2 Fenton F, Cherry E. Models of cardiac cell. Scholarpedia, 2008, 3: 1868
3 Fink M, Niederer S A, Cherry E M, et al. Cardiac cell modelling: observations from the heart of the cardiac physiome project. Prog Biophys Mol Biol, 2011, 104: 2–21
4 Moreno J D, Zhu Z I, Yang P C, et al. A computational model to predict the effects of class i anti-arrhythmic drugs on ventricular rhythms. Sci Transl Med, 2011, 3: 98ra83
5 Clayton R H, Bernus O, Cherry E M, et al. Models of cardiac tissue electrophysiology: progress, challenges and open questions. Prog Biophys Mol Biol, 2011, 104: 22–48
6 Quarteroni A, Manzoni A, Vergara C. The cardiovascular system: mathematical modelling, numerical algorithms and clinical applications. Acta Numerica, 2017, 26: 365–590
7 Jalife J. Introduction to the series on computational approaches to cardiac arrhythmias. Circ Res, 2013, 112: 831–833
8 Trayanova N A, Chang K C. How computer simulations of the human heart can improve anti-arrhythmia therapy. J Physiol, 2016, 594: 2483–2502
9 Arevalo H J, Vadakkumpadan F, Guallar E, et al. Arrhythmia risk stratification of patients after myocardial infarction using personalized heart models. Nat Commun, 2016, 7: 11437
10 Kaboudian A, Cherry E M, Fenton F H. Real-time interactive simulations of large-scale systems on personal computers and cell phones: toward patient-specific heart modeling and other applications. Sci Adv, 2019, 5: eaav6019
11 Grandi E, Pasqualini F S, Puglisi J L, et al. A novel computational model of the human ventricular action potential and Ca transient. Biophys J, 2009, 96: 664–665
12 O'Hara T, Virág L, Varró A, et al. Simulation of the undiseased human cardiac ventricular action potential: model formulation and experimental validation. PLoS Comput Biol, 2011, 7: e1002061
13 Ten Tusscher K H W J, Noble D, Noble P J, et al. A model for human ventricular tissue. Am J Physiol-Heart Circul Physiol, 2004, 286: H1573–H1589
14 Ten Tusscher K H W J, Panfilov A V. Alternans and spiral breakup in a human ventricular tissue model. Am J Physiol-Heart Circul Physiol, 2006, 291: H1088–H1100
15 Niederer S A, Smith N P. At the heart of computational modelling. J Physiol, 2012, 590: 1331–1338
16 Noble D. Modeling the heart—from genes to cells to the whole organ. Science, 2002, 295: 1678–1682
17 Noble D. The rise of computational biology. Nat Rev Mol Cell Biol, 2002, 3: 459–463
18 Lara-Benítez P, Carranza-García M, Riquelme J C. An experimental review on deep learning architectures for time series forecasting. Int J Neur Syst, 2021, 31: 2130001
19 Kashinath K, Mustafa M, Albert A, et al. Physics-informed machine learning: case studies for weather and climate modelling. Phil Trans R Soc A, 2021, 379: 20200093
20 Pfaff T, Fortunato M, Sanchez-Gonzalez A, et al. Learning mesh-based simulation with graph networks. In: Proceedings of the International Conference on Learning Representations, 2020
21 Reichstein M, Camps-Valls G, Stevens B, et al. Deep learning and process understanding for data-driven Earth system science. Nature, 2019, 566: 195–204
22 Li Y, Wan R, Liu J, et al. In silico mechanisms of arsenic trioxide-induced cardiotoxicity. Front Physiol, 2022, 13: 1004605
23 Fox J J, McHarg J L, Gilmour Jr R F. Ionic mechanism of electrical alternans. Am J Physiol-Heart Circul Physiol, 2002, 282: H516–H530
24 Goldhaber J I, Xie L H, Duong T, et al. Action potential duration restitution and alternans in rabbit ventricular myocytes. Circ Res, 2005, 96: 459–466
25 Kalb S S, Dobrovolny H M, Tolkacheva E G, et al. The restitution portrait: a new method for investigating rate-dependent restitution. Cardiovasc Electrophysiol, 2004, 15: 698–709
26 Fan W, Zheng S, Yi X, et al. Depts: deep expansion learning for periodic time series forecasting. In: Proceedings of the 10th International Conference on Learning Representations, 2022
27 Cavero I, Holzgrefe H. CiPA: ongoing testing, future qualification procedures, and pending issues. J Pharmacol Toxicol Methods, 2015, 76: 27–37
28 Dutta S, Chang K C, Beattie K A, et al. Optimization of an in silico cardiac cell model for proarrhythmia risk assessment. Front Physiol, 2017, 8: 616
29 Liu Y, Li D, Nie D, et al. Arsenic trioxide and angiotensin II have inhibitory effects on HERG protein expression: evidence for the role of PML SUMOylation. Oncotarget, 2017, 8: 45447–45458
30 Alexandre J, Moslehi J J, Bersell K R, et al. Anticancer drug-induced cardiac rhythm disorders: current knowledge and basic underlying mechanisms. Pharmacol Ther, 2018, 189: 89–103
31 Ducas R A, Seftel M D, Ducas J, et al. Monomorphic ventricular tachycardia caused by arsenic trioxide therapy for acute promyelocytic leukaemia. J R Coll Phys Edinburgh, 2011, 41: 117–118
32 Chen X, Shan H, Zhao J, et al. L-type calcium current ($I_{\mathrm{Ca,L}}$) and inward rectifier potassium current ($I_{\mathrm{K1}}$) are involved in QT prolongation induced by arsenic trioxide in rat. Cell Physiol Biochem, 2010, 26: 967–974

33 Yan M, Feng L, Shi Y, et al. Mechanism of $As_2O_3$-induced action potential prolongation and using hiPS-CMs to evaluate the rescue efficacy of drugs with different rescue mechanism. Toxicol Sci, 2017, 158: 379–390
34 Sobie E A. Parameter sensitivity analysis in electrophysiological models using multivariable regression. Biophys J, 2009, 96: 1264–1274
35 Whittaker D G, Clerx M, Lei C L, et al. Calibration of ionic and cellular cardiac electrophysiology models. WIREs Mech Dis, 2020, 12: e1482
36 Benson A P, Stevenson-Cocks H J, Whittaker D G, et al. Multi-scale approaches for the simulation of cardiac electrophysiology: II-tissue-level structure and function. Methods, 2021, 185: 60–81
37 Amorim E, Zheng W L, Ghassemi M M, et al. The international cardiac arrest research consortium electroencephalography database. Crit Care Med, 2023, 51: 1802–1811
38 Goldberger A L, Amaral L A N, Glass L, et al. Physiobank, physiotoolkit, and physionet. Circulation, 2000, 101: 215–220
39 Wajdan A, Jahren T S, Villegas-Martinez M, et al. Automatic detection of aortic valve events using deep neural networks on cardiac signals from epicardially placed accelerometer. IEEE J Biomed Health Inform, 2022, 26: 4450–4461